Applied Catalysis B: Environmental 138–139 (2013) 62–69

Contents lists available at SciVerse ScienceDirect

Applied Catalysis B: Environmental

journal homepage: www.elsevier.com/locate/apcatb

A photo-catalysis and rotating nano-$CaCO_3$ dynamic membrane system with Fe-$ZnIn_2S_4$ efficiently removes halogenated compounds in water

Bo Gao, Lifen Liu*, Jiadong Liu, Fenglin Yang

Key Laboratory of Industrial Ecology and Environmental Engineering, MOE, School of Environmental Science and Technology, Dalian University of Technology, Dalian 116024, PR China

ARTICLE INFO

Article history:
Received 1 December 2012
Received in revised form 19 January 2013
Accepted 3 February 2013
Available online 26 February 2013

Keywords:
Photocatalytic membrane reactor
Dynamic membrane
2,4,6-Tribromophenol
2,4-Dichlorophenol

ABSTRACT

A photo-catalysis and dynamic membrane reactor system (PMR), with coated nano$CaCO_3$ layer on polypropylene non-woven fabric material, was studied for continuous photocatalysis and retention of catalysts in a single device, in removing halogenated compounds (2,4,6-Tribromophenol and 2,4-Dichlorophenol) in water. Both the batch and the continuous photocatalytic experiments were carried out to investigate the efficiency in COD removal, in removing halogenated compounds and in dehalogenation. A comparison of the separation performance of photocatalysts between bare (uncoated) and pre-coated nano$CaCO_3$ dynamic membranes was conducted. The pre-coated dynamic membrane can significantly enhance the filtration performance and improve the retention of photocatalysts. Particularly, nano$CaCO_3$ was found able to assist and improve debromination efficiency during UV irradiated photolysis. Tentative debromination pathway and dehalogenation mechanism were proposed. Due to the assisted additional reaction by the nano$CaCO_3$ dynamic membrane, the PMR system with nano$CaCO_3$-coating and Fe-$ZnIn_2S_4$ completely removed halogenated compounds, achieved highest COD removal (72% for 2,4,6-Tribromophenol and 75% for 2,4-Dichlorophenol), 85–90% debromination and 99% dechlorination efficiencies. The long-term continuous photocatalytic debromination experiments demonstrated that the dynamic membrane hybrid system was very steady in the long-term operation and the debromination maintained at about 85% during the 40 h photocatalytic debromination reaction. The combination of dynamic membrane and photocatalysis provides a new alternative for practical application of photocatalysis.

1. Introduction

Photocatalysis is a promising alternative advanced oxidation process for water and wastewater treatment, especially it can achieve effective degradation of low concentration, high toxic organic pollutants such as chlorophenols [1–3] and bromophenols [4,5]. Photocatalysts were often used in the form of nanoparticles in suspension slurries [6–8] to remove contaminants in water, since suspend catalysts allowed much better contact between the catalysts and pollutants, and had higher efficiency than the immobilized catalysts [9]. However, the major concern for the practical application of photocatalytic technology is the separation of the suspended photocatalysts. Application of a hybrid membrane with both immobilized and suspended catalyst systems, the so called "photocatalytic membrane reactor" (PMR) [10], is an applicable and promising approach which could not only overcome the difficulty in separating photocatalysts but also could integrate photocatalytic degradation of contaminants and membrane separation. Many researches about immobilizing photocatalysts on both inorganic [11,12] and organic membrane [13–15] substrates had been carried out. But, the immobilized photocatalyst can only be partly used and only one side of the fixed-membrane can be illuminated, which reduced the quantum efficiency, thus fine-powder catalyst suspension in a membrane system has been investigated.

The commonly used suspend photocatalysts were nanoscale particles, therefore, for high retention rate of catalysts, pressure driven membrane processes such as MF [16], UF [13] and NF [17] were applied. However, the membrane fouling caused by nanocatalysts particles was the main limiting factor that hindered the implementation of membrane technologies in separating fine particles in suspension. The fouling mechanism of hollow fiber membranes in separating nanosized photocatalysts was associated with pore blocking and cake layer formation, also, hydrodynamic back flush was unable to completely eliminate the filtration resistance due

Abbreviations: PMR, photocatalytic membrane reactor; 2,4,6-TBP, 2,4,6-Tribromophenol; 2,4-DCP, 2,4-Dichlorophenol.

* Corresponding author. Tel.: +86 411 84706173; fax: +86 411 84708083.
E-mail address: yuzhe25521@yahoo.com.cn (L. Liu).

0926-3373/$ – see front matter © 2013 Elsevier B.V. All rights reserved.
http://dx.doi.org/10.1016/j.apcatb.2013.02.023

to the adhesion of nanosized catalysts [18]. Moreover, when polymer membranes were used, there was a danger of degradation and destruction of the membrane structure by UV light or hydroxyl radicals [19]. Several studies [6,20,21] reported that the combination of membrane separation and photocatalysis in separating photocatalyst nanoparticles in two independent operation processes. After photocatalytic reaction, membrane filtration was performed to recover photocatalysts and the rejected photocatalysts were mixed with influent to realize the continuous photocatalytic reaction. This approach may increase the operational complexity and the frequent back-pulsing may increase the cost in practicable application.

Dynamic membrane [22], which is called secondary membrane, is formed on underlying support material by filtering suspended solid particles. It is anticipated that the hybrid dynamic membrane and photocatalysis system can reduce irreversible membrane fouling, enhance photocatalytic activity and protect organic membrane from destruction by photocatalysis. The pre-coated iron oxide particles (IOPs) layer on the hollow fiber MF membrane surface was formed by suction of IOPs solution and then the dynamic membrane was employed in the photocatalysis-microfiltration hybrid system for the removal of natural organic matter in water [8]. The rejection properties of the dynamic membrane mainly depend on the deposited layer, since solids rejection is accomplished by the self-forming and/or pre-coated secondary membrane layer. The dynamic membrane can separate fine particles even though the support membrane has large pore size. Therefore, different kinds of low-cost materials such as non-woven fabric and woven filter-cloth can be used as supporting membrane instead of expensive ultrafiltration (UF) and/or nanofiltration (NF) membranes. The pre-coated dynamic membranes are generally formed from added powder materials in a single step. The commonly used dynamic layer forming powders are inorganics, especially metal oxides such as TiO_2 [23], Kaolin/MnO_2 bi-layer [24].

$CaCO_3$, as a cheap and stable naturally occurring mineral, is widely used in industrial manufacturing, construction, pharmaceutical and cosmetic industry. It is anticipated that $CaCO_3$, especially the 'nanosized' $CaCO_3$, a good candidate for forming dynamic membrane layer on non-woven fabric membrane, would enhance the filtration performance in photocatalysis-membrane hybrid system.

The combination of rotating dynamic membrane and photocatalysis is expected to show many advantages, like: (1) the investment and operational costs are expected to be lower than the conventional expensive ultrafiltration (UF) and/or nanofiltration (NF) membranes and even the inorganic ceramic membrane; (2) the hybrid system can realize continuous photocatalysis, stirring and separation of photocatalysts in a single device which simplified the operational complexity; (3) the precoated inorganic $CaCO_3$ cake layer can prevent fouling of supporting membrane; (4) the precoated inorganic $CaCO_3$ cake layer can protect the organic membrane from destruction.

The purpose of this study was to investigate the photocatalytic debromination of 2,4,6-Tribromophenol (2,4,6-TBP) and dechlorination of 2,4-Dichlorophenol (2,4-DCP) in a hybrid photocatalysis and dynamic membrane system, with a pre-coated $CaCO_3$ dynamic layer on non-woven fabric supporting helical membrane. Rotating the helical membrane module can serve as a stirrer to ensure the uniform suspension of photocatalysts and uniform illumination of photocatalysts. The self-prepared zerovalent iron doped $ZnIn_2S_4$ was proved to be very efficient in debromination of 2,4,6-TBP in our recent research [25] and used as an efficient photocatalytic dehalogenation catalyst. The dehalogenation and mineralization efficiency in batch and continuous mode were evaluated, and compared with TiO_2. The long-term photocatalytic debromination was carried out to evaluate the stability of this photocatalysis/dynamic membrane system and to explore its practical application possibility.

2. Experimental

2.1. Materials

2,4,6-Tribromophenol (2,4,6-TBP, AR) and 2,4-Dichlorophenol (2,4-DCP, AR) were supplied by Sinpharm Chemical Reagent Co., Ltd. The initial concentration of 2,4,6-TBP was 40 mg l^{-1} and the initial pH was 6.89. The concentration of 2,4-DCP was 15 mg l^{-1} and the initial unadjusted pH was 7.20. Other reagents such as $Zn(NO_3)_2{\cdot}6H_2O$, $In(NO_3)_3{\cdot}5H_2O$, CH_3CSNH_2 (TAA), $FeSO_4{\cdot}7H_2O$ and $NaBH_4$ are all of analytical grade. The commercial Degussa P25 was used as the standard TiO_2 sample. Nanoscale $CaCO_3$ (Xintai Nanometer Material Co., Ltd.), with a cluster size of ~24 μm (determined by Mastersizer 2000, Malvern) and individual particle size 50–100 nm (from TEM image), was used as the dynamic layer forming material. The common $CaCO_3$ (analytical grade) was tested as comparison. Polypropylene non-woven fabric without modification, with a pore size of 3–5 μm and weight per unit area at 5.0 g m^{-2}, was employed as underlying support membrane. All materials were used as received without further purification. The water used in the tests was deionized water.

2.2. Preparation of nano$CaCO_3$ dynamic membrane

The helical membrane with 180° helical angle, prepared the same way as in our previous research [26], was used as the supporting membrane. Two pieces of the non-woven fabric sheets (20 mm × 230 mm × 2 mm, total area 0.0092 m^2) were supported on an aluminum mesh spacer to maintain the helical angle. The wire diameter of the aluminum spacer is 0.5 mm. The cover membrane was sealed and connected with a tubing outlet at one end of the membrane to conduct the permeate water out.

The non-woven fabric helical membrane was immersed in 5.0 g l^{-1} $CaCO_3$ solution. The $CaCO_3$ coating layer was formed by suction (−9.1 kPa), and $CaCO_3$ loading was 0.014 g cm^{-2} on the helical membrane surface. Then the coating layer was further aged and stabilized for 1 h under the pressure. No $CaCO_3$ particles were released when the helical dynamic membrane was rotated at a rotating speed of 75 rpm, thus the formed $CaCO_3$ precoating layer was stably maintained during the photocatalysis in this rotating helical membrane system. Then, the dynamic membrane was used for continuous and efficient photocatalytic degradation of 2,4,6-TBP and 2,4-DCP, after adding photocatalyst powder to this photocatalysis and membrane system (PMR).

2.3. Photocatalytic activity measurements

The zero valent iron doped $ZnIn_2S_4$ photocatalyst with a mass ratio of 0.5% Fe^0, prepared in the laboratory according to our recent research [25], was applied as the dehalogenation photocatalyst. The photocatalytic reactions were carried out in batch mode for suspended photocatalysts and continuous mode in PMR system.

In batch tests, the Fe-$ZnIn_2S_4$, TiO_2, nanoscale $CaCO_3$ or common $CaCO_3$ powder samples were tested in the adsorption or degradation of 2,4,6-TBP and 2,4-DCP in the dark or under UV irradiation. A mass weight of 100 mg of the catalyst powder (TiO_2, Fe (0.5%)-$ZnIn_2S_4$) or nanoscale $CaCO_3$ and common $CaCO_3$ and 100 ml of 2,4,6-TBP or 2,4-DCP solution were added into the quartz reactor from the top portion of the tube and subjected to aeration (0.1 l min^{-1}) for thorough mixing and suspension. Samples of 5.0 ml reaction suspension was withdrawn at specific time intervals and filtered through 0.22 μm millipore (acetate cellulose) filter and then analyzed for concentration measurements of 2,4,6-TBP, 2,4-DCP and the released Br^- and/or Cl^-. After 2 h reaction, samples were collected and centrifuged at 12,000 rpm for 10 min to get the

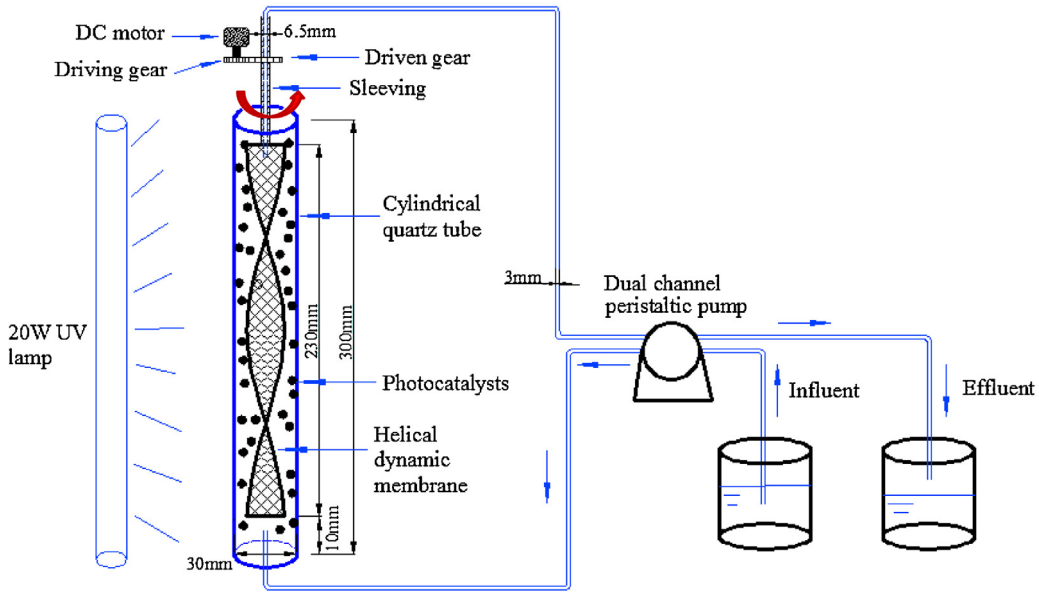

Fig. 1. A schematic of the laboratory scale photocatalysis-helical dynamic membrane hybrid system.

supernatant for measuring the extent of mineralization of 2,4,6-TBP and 2,4-DCP.

In the continuous tests with the PMR system (Fig. 1), the helical nanoscale $CaCO_3$ coated membrane was submerged in the 2,4,6-TBP or 2,4-DCP solution. Fe-doped $ZnIn_2S_4$ and TiO_2 were applied as dehalogenation photocatalysts and the photocatalyst dosage was 1.0 g l^{-1}. The continuously rotating helical dynamic membrane, serving as the stirrer to maintain photocatalysts in suspension, was operated under constant flux of 7.6 l m^{-2} h^{-1}. The helical membrane module rotated counterclockwise. The residence time of 2,4,6-TBP or 2,4-DCP solution in the reactor was maintained at 2.0 h. The influent and effluent flows were controlled through a dual channel peristaltic pump (Baoding Longer Precision Pump Co., Ltd.) to maintain the liquid suspension level at about 140 ml. The permeate samples were collected for measuring the concentration of 2,4,6-TBP or 2,4-DCP, COD_{Mn} and the released Cl^- or Br^-. In addition, the separation effectiveness of photocatalysts (Fe-$ZnIn_2S_4$ and TiO_2) by dynamic membrane and bare membrane was determined and compared by turbidity removal.

The photocatalytic cylindrical quartz tube reactor used for both batch and continuous tests has a dimension of 3.0 cm × 30 cm (diameter × height). The light source was positioned at one side of the cylindrical quartz tube. The distance between the reactor and the lamp was 10 cm. The UV light source was a 20 W germicidal low-pressure mercury lamp with main wavelength of 254 nm and the light intensity was 297 μW cm^{-2} (with Al reflector surrounding the reactor and the lamp).

The concentration of 2,4,6-TBP was determined using high performance liquid chromatography (HPLC, Shimadzu, VP-ODS, 150 L × 4.6), in which a mobile phase of methanol and water was employed (80:20, v/v) at a flow rate of 1.0 ml min^{-1}, an injection volume of 5 μl was used and the UV detector wavelength was set at 295 nm. The concentration of 2,4-DCP was determined also with a mobile phase of methanol and water (60:40, v/v) at a flow rate of 1.0 ml min^{-1} and the UV detector wavelength was 284 nm.

The released Br^- was measured according to the method for determining bromide content in groundwater (F-HZ-DZ-DXS-0062, China). The released Cl^- concentration and COD_{Mn} were measured according to standard methods for the examination of water and wastewater (American Public Health Association, 2005). The data reported were average of three tests and the error bars represented the standard deviation.

The ultraviolet-visible spectrophotometer (Shimadzu, UV-1700) was used to detect the changes of phenol during the process. Turbidity was measured using a PGENERAL T6 visible light spectrophotometer. The liquid chromatography–electron spray ionization mass spectrometry (LC–ESI-MS, Agilent Technologies) was used to determine the debromination intermediates. Chromatographic analysis was carried out with a mixture of 40% ultrapure water supplemented with 0.2% formic acid and 60% acetonitrile. The flow rate was 0.25 ml min^{-1} and 5.0 μl of the extracted samples were injected.

2.4. The long-term photocatalytic debromination

The long-term continuous photocatalytic debromination was carried out to evaluate the stability of the photocatalyst and the photocatalysis/dynamic membrane system. 1.0 g l^{-1} Fe doped $ZnIn_2S_4$ was applied as debromination photocatalyst. The long-term continuous test was carried out in the nano$CaCO_3$ dynamic membrane and photocatalysis system, and the residence time of 2,4,6-TBP was maintained at 2.0 h. The photocatalytic reaction was continued for 10 h during daytime and discontinued at night. And then the experiment was maintained for another 10 h during the second daytime. In this way, the experiment lasted for 80 h without catalyst replacement. The permeate was collected for measuring the concentration of 2,4,6-TBP and the released bromide content at 1.0 h time interval.

3. Results and discussion

3.1. Batchwise photocatalytic dehalogenation of 2,4,6-TBP and 2,4-DCP

In order to evaluate the photocatalytic dehalogenation in suspension system, a series of comparison experiments with Fe-$ZnIn_2S_4$, TiO_2, nanoscale $CaCO_3$ and common $CaCO_3$ powder samples were carried out in adsorption and/or degradation of 2,4,6-TBP and 2,4-DCP in the dark and/or under UV irradiation.

The results of adsorption experiments (Fig. S1) showed that the adsorption capacity was low for TiO_2 and nanoscale $CaCO_3$ powder samples and only ~20% 2,4,6-TBP was removed after 2.0 h adsorption in the dark. About 55% 2,4,6-TBP was removed by Fe-$ZnIn_2S_4$ after 2.0 h adsorption, which might be related to the BET surfaces

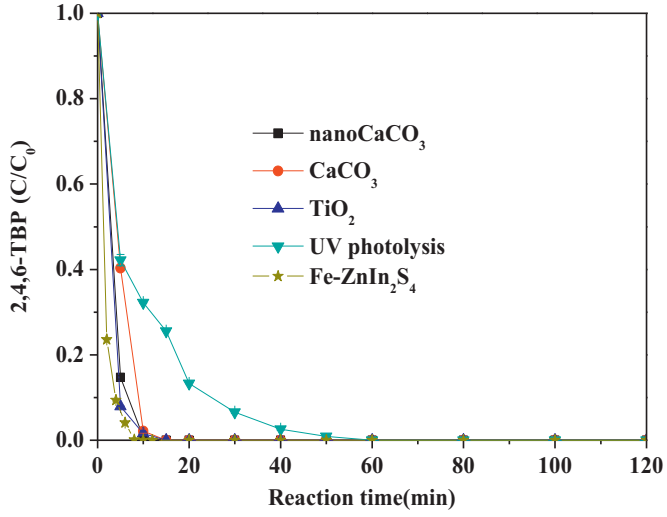

Fig. 2. Photodebromination of 2,4,6-TBP by nanoCaCO$_3$, CaCO$_3$, TiO$_2$ and 0.5 wt% Fe-ZnIn$_2$S$_4$ ([2,4,6-TBP]$_0$ = 40 mg l^{-1}, pH 6.89, catalyst dosage = 1.0 g l^{-1}, 20 W low-pressure mercury lamp (light intensity was 297 μW cm^{-2})).

and morphology of the catalysts that had been discussed in our previous research [25].

Without any photocatalysts, 2,4,6-TBP was found eliminated after 1.0 h UV irradiation (Fig. 2), which was considered preliminary degradation. Pollutant 2,4,6-TBP can be easily transformed to quinones intermediates in the presence of UV irradiation. It was observed that 2,4,6-TBP was rapidly transformed to its lower degree substituted bromo congeners and/or quinones intermediates, but, it was difficult for further debromination and mineralization. It was further proved by the determined concentration of the released bromide ion (Br^-). The C/C_{100} ratios of Br^- for different catalysts were shown in Fig. 3. C_{100} of bromide was defined here as the Br^- concentration at 100% debromination and C represented the released bromide concentration. Only 30% bromide was released after 2.0 h direct UV photolysis.

In Fig. 2, 2,4,6-TBP was not detected after 15 min irradiation in the reaction system containing TiO$_2$. Moreover, rapid degradation of 2,4,6-TBP occurred in the presence of Fe-ZnIn$_2$S$_4$ under UV irradiation and 2,4,6-TBP completely disappeared after 8 min irradiation. After 2.0 h photocatalytic reaction by Fe-ZnIn$_2$S$_4$, the released Br^- concentration was ~25 mg l^{-1} corresponding to 88% debromination, which was 1.4 times higher than TiO$_2$ (P25). The debromination pathway and photocatalytic mechanism had been proposed in our previous study.

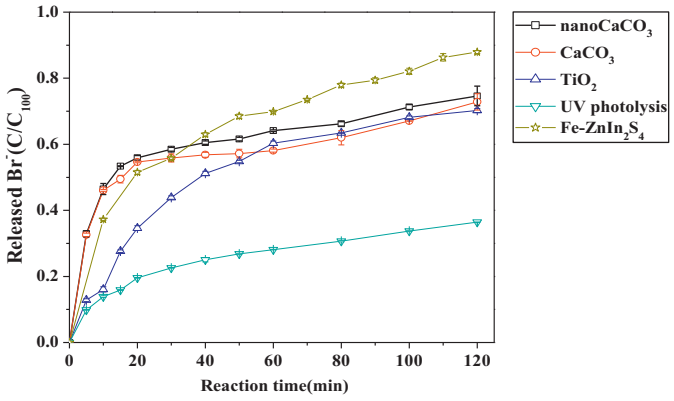

Fig. 3. The released Br^- concentration for different catalysts (C_{100} of bromide was determined as the Br^- concentration at 100% debromination (C_{100} = 29 mg l^{-1}) and C represented the released bromide concentration).

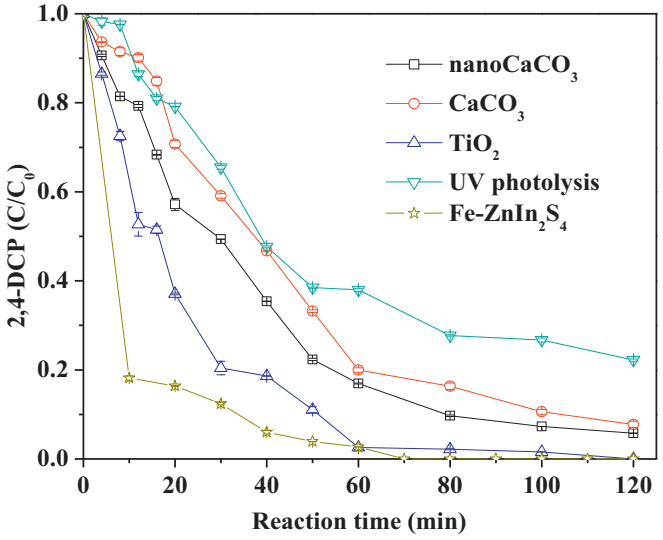

Fig. 4. Photodechlorination of 2,4-DCP by nanoCaCO$_3$, CaCO$_3$, TiO$_2$ and 0.5 wt% Fe-ZnIn$_2$S$_4$ ([2,4-DCP]$_0$ = 15 mg l^{-1}, catalyst dosage = 1.0 g l^{-1}, 20 W low-pressure mercury lamp (light intensity was 297 μW cm^{-2})).

Unexpectedly, 2,4,6-TBP in CaCO$_3$ and nanoCaCO$_3$ dispersions was rapidly degraded by UV irradiation and after 10 min, the elimination was complete. From the released bromide concentration in Fig. 3, the debromination occurred much more quickly in the presence of CaCO$_3$ and/or nanoCaCO$_3$ at the initial stage and debromination was 60% within 30 min, then the debromination rate slowed down and reached 67% debromination after 2.0 h irradiation, which was a little higher than the photocatalytic debromination by TiO$_2$ (63%). This indicated that CaCO$_3$ and/or nanoCaCO$_3$ assisted UV irradiated photolysis/photocatalysis and improved degradation and debromination efficiency of 2,4,6-TBP, which had not been reported previously to our best knowledge. This might be caused by the increased light use and high quantum efficiency because of the effect of CaCO$_3$ in scattering and slowing down the incident light, and in adsorbing the pollutant molecules to the surface of CaCO$_3$, molecules in adsorbed state may be degraded differently (rate and route) than photolysis in solution phase. The detailed proposed debromination mechanism will be discussed in the next section.

The degradation of 2,4-DCP in CaCO$_3$ and/or nanoCaCO$_3$ dispersions was also carried out under UV irradiation. The 2,4-DCP degradation tendency in Fig. 4 was similar to that of 2,4,6-TBP, and more than 94% 2,4-DCP was degraded under 2.0 h UV irradiation. In contrast, the direct photolysis degraded 77% 2,4-DCP and adsorption only removed 30% 2,4-DCP (Fig. S2).

The kinetics of dehalogenation of 2,4,6-TBP and 2,4-DCP was fitted using a pseudo-first-order process, the obtained rate constants were listed in Table 1. It was obvious that the pseudo-first-order rate constants for 2,4,6-TBP debromination were much bigger than

Table 1
The pseudo-first-order rate constants for debromination of 2,4,6-TBP and dechlorination of 2,4-DCP in the presence of UV light ([2,4,6-TBP]$_0$ = 40 mg l^{-1}, [2,4-DCP]$_0$ = 15 mg l^{-1}, catalysts dosage = 1.0 g l^{-1}).

Catalysts	Pseudo-first-order rate constant K_r (min^{-1})			
	2,4-DCP	R^2	2,4,6-TBP	R^2
NanoCaCO$_3$	0.02656	0.9721	0.4933	0.9650
Common CaCO$_3$	0.02328	0.9783	0.4015	0.9169
TiO$_2$	0.04456	0.9525	0.4304	0.9779
0.5 wt% Fe-ZnIn$_2$S$_4$	0.08267	0.9139	0.6558	0.9679
UV photolysis	0.01296	0.9219	0.0885	0.9889

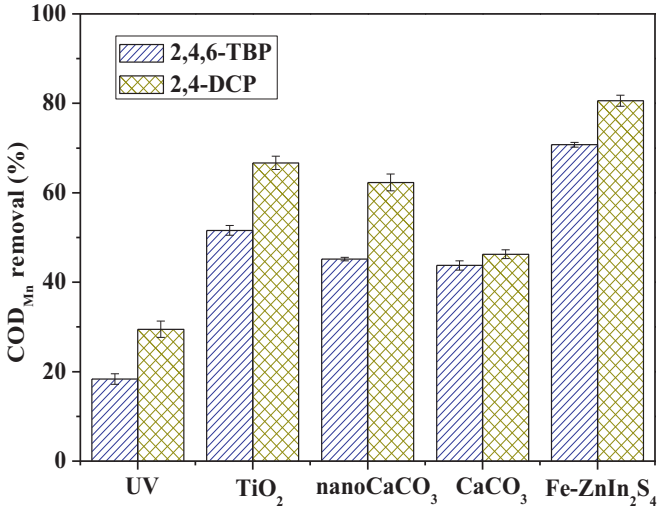

Fig. 5. COD_{Mn} removal for 2,4,6-TBP and 2,4-DCP by different catalysts after 2.0 h reaction ($[2,4,6\text{-TBP}]_0 = 40\ mg\ l^{-1}$, pH 6.89, $[2,4\text{-DCP}]_0 = 15\ mg\ l^{-1}$ catalyst dosage = $1.0\ g\ l^{-1}$, 20 W low-pressure mercury lamp).

that of 2,4-DCP dechlorination. This can be attributed to the difference in the bond energy of C—Br in 2,4,6-TBP and C—Cl in 2,4-DCP. The bond energy of C—Cl (399.6 ± 6.3 kJ/mol) is much stronger than C—Br bond (349.4 ± 10.5 kJ/mol), therefore, it would be more difficult to break C—Cl bond in 2,4-DCP and thus the dechlorination of 2,4-DCP was more slow than debromination of 2,4,6-TBP. The pseudo-first-order rate constants for 2,4,6-TBP debromination in the presence of $CaCO_3$ (0.401) and/or nano$CaCO_3$ (0.493) were at the same level as photocatalytic debromination by TiO_2 (0.430).

COD removal is considered an important indicator in evaluating the mineralization degree and toxicity reduction of the organic pollutants. After debromination and dechlorination, the cleavage of the benzene ring followed, and the generated carbon species were subsequently degraded, which led to complete mineralization later on. In Fig. 5, it was observed that Fe-$ZnIn_2S_4$ achieved highest COD removal and 70% COD for 2,4,6-TBP and 80% COD for 2,4-DCP were removed after 2.0 h reaction. The COD removal for 2,4,6-TBP and 2,4-DCP degradation in the presence of nano$CaCO_3$ were 45% and 62%, respectively, which was comparable with the COD removal by TiO_2 photocatalytic degradation (50% for 2,4,6-TBP and 66% for 2,4-DCP). The debromination and dechlorination experiments demonstrated that nano$CaCO_3$ and/or $CaCO_3$ in the presence of UV irradiation could improve the degradation of halogenated pollutants and also enhance the dehalogenation efficiency, while, the mechanism was not clear yet.

3.2. Debromination pathway and dehalogenation mechanism assisted by nano$CaCO_3$ under UV irradiation

3.2.1. Characterization of $CaCO_3$

Transmission electron microscopy (TEM-100CX-II) and high-resolution TEM (HRTEM) analyses of nano$CaCO_3$ were operated at an accelerating voltage of 200 kV. It was observed that $CaCO_3$ showed a cubic structure with an average cube edge of over 50–100 nm (Fig. S3a). The lattice interplanar spacing measured at HRTEM image (Fig. S3b) was ~0.306 nm, corresponding to the (1 0 4) crystal plane of calcite phase [27]. The crystallographic structure and phase of nano$CaCO_3$ and common $CaCO_3$ samples were identified by XRD. As shown in Fig. S4, every diffraction peak was in well agreement with the standard diffraction patterns of calcite [27]. The optical property of nano$CaCO_3$ was measured by a UV-Vis spectrophotometer (JASCO Corp., V-550) and TiO_2 was measured for comparison. For nano$CaCO_3$, there was a little absorbency observed in the range of UV region (Fig. S5) and the absorption intensity was not as intense as TiO_2. All the characterizations demonstrated that there was no big difference between nano$CaCO_3$ and common $CaCO_3$ except for the particle size and they were regarded as the common calcite.

3.2.2. Debromination pathway of 2,4,6-TBP in the presence of nano$CaCO_3$ under UV irradiation

In order to figure out the degradation mechanism and degradation pathway, the debromination of 2,4,6-TBP by nano$CaCO_3$ was carried out under UV irradiation, the intermediate products resulting from 2,4,6-TBP degradation at 10 min, 30 min, 60 min and 120 min were analyzed using HPLC–ESI-MS.

According to results in Fig. 6, the characteristic peak of 2,4,6-TBP at m/z 328.8 was not detected and 100% 2,4,6-TBP was transformed within 10 min. The results revealed that 2,4,6-TBP was completely degraded and simultaneously transformed to the detected main intermediates. Two main intermediate products at m/z 186.9 and m/z 266.8 were detected after 10 min reaction, which probably corresponded to 2-Bromo-1,4-Benzoquinone and 2,6-Dibromo-P-Benzoquinone, respectively. The relative intensity of 2,6-Dibromo-P-Benzoquinone decreased along with the irradiation time and disappeared completely after 60 min reaction (Table S1). And the intermediate 2-Bromo-1,4-Benzoquinone was also reduced with the prolonged reaction time and completely decomposed after 2.0 h reaction.

It has been proposed that quinones were formed as the main intermediates during the oxidative dehalogenation of 2,4,6-trichlorophenol [2]. On the basis of the identified intermediates, the quinones (2,6-Dibromo-P-Benzoquinone and 2-Bromo-1,4-Benzoquinone) made up a large part of the intermediates, which indicated that the oxidative debromination played a leading role in the debromination of 2,4,6-TBP. Therefore, we proposed that the degradation of 2,4,6-TBP by nano$CaCO_3$ under UV irradiation started with oxidative debromination.

3.2.3. Dehalogenation mechanism

$CaCO_3$ is not semiconductor so that photocatalytic mechanism seemed inappropriate for debromination and dechlorination in the presence of nano$CaCO_3$ under UV irradiation. The most possible mechanism might be that the regular distribution calcium carbonate structure (SEM image) could scatter and slow the incident light and make it distribute uniformly [28], which could increase light utilization and quantum efficiency. It was presumed that the enhanced debromination and dechlorination were accomplished by the increased direct UV photolysis in the solution and on the $CaCO_3$ surface. The shape of the debromination curves in the presence of $CaCO_3$ and nano$CaCO_3$ was similar to the shape of the curve of direct photolysis, except that the debromination increased many folds (Fig. 3), which indicated that the debromination in the presence of $CaCO_3$ might undergo the same reaction mechanism as direct photolysis. Fine particles of nano$CaCO_3$ cause more increase in light use and photolysis, so that nano$CaCO_3$ exhibited better activity than common $CaCO_3$ in degrading of 2,4,6-TBP and 2,4-DCP. Nano$CaCO_3$ function as light slow-down and scatter media in debromination and dechlorination under UV irradiation. The direct UV photolysis of 2,4,6-TBP (Fig. 2) and 2,4-DCP (Fig. 4), especially the photolysis of adsorbed molecules, plus the increase of light use efficiency caused by nano$CaCO_3$ particles, resulted in rapid degradation of 2,4,6-TBP and 2,4-DCP and significant increase of debromination.

Taking advantage of the enhanced dehalogenation by nano$CaCO_3$ under UV irradiation, a pre-coated nano$CaCO_3$ dynamic membrane was integrated in continuous photocatalysis and efficient dehalogenation of 2,4,6-TBP and 2,4-DCP. Nanosized $CaCO_3$ is expected to play several roles in the membrane reactor, as

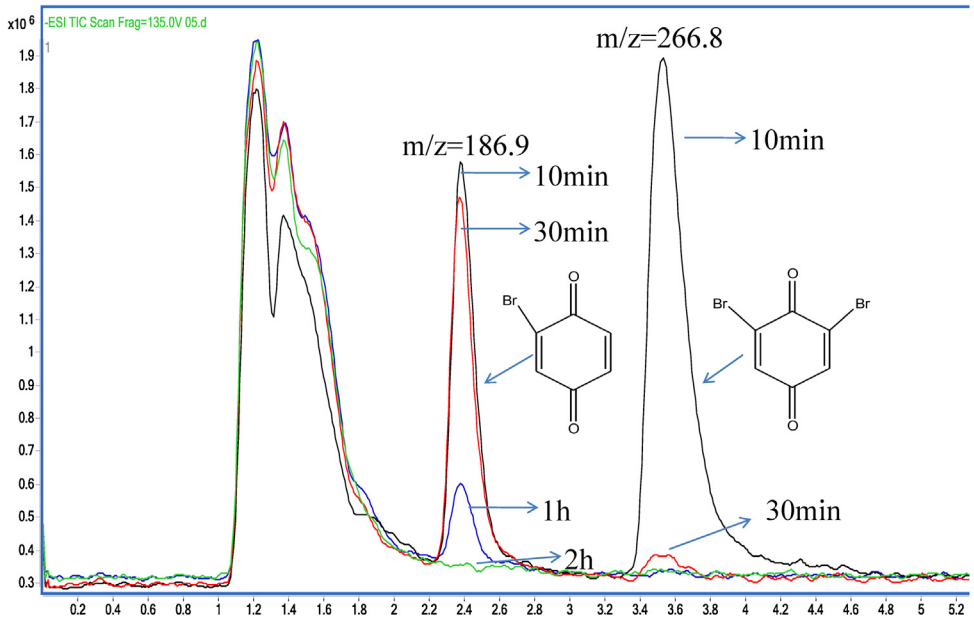

Fig. 6. The intermediate products resulting from 2,4,6-TBP degradation at 10 min, 30 min, 60 min and 120 min were analyzed using HPLC–ESI-MS.

follows: (1) the precoated $CaCO_3$ cake layer on non-woven fabric supporting membrane can significantly enhance the filtration performance and improve the rejection of both TiO_2 and Fe-$ZnIn_2S_4$; (2) $CaCO_3$ is expected to assist and enhance dehalogenation and mineralization efficiency; (3) the precoated inorganic $CaCO_3$ cake layer can prevent fouling of supporting membrane and protect the organic membrane from destruction.

3.3. Continuous photocatalytic dehalogenation in dynamic membrane and photocatalysis system

3.3.1. Pre-coated nano$CaCO_3$ dynamic membrane system

The gravitational suction permeation was adopted in pre-coating nano$CaCO_3$ dynamic layer and the TMP across the helical membrane was maintained at ~9.1 kPa. The permeate flux and turbidity variation in the pre-coating stage was shown in Fig. 7. It can be observed that the permeate flux dropped rapidly from 27 l m^{-2} h^{-1} kPa^{-1} to 17 l m^{-2} h^{-1} kPa^{-1} in the first 10 min, then decreased slowly and maintained at about 11 l m^{-2} h^{-1} kPa^{-1}.

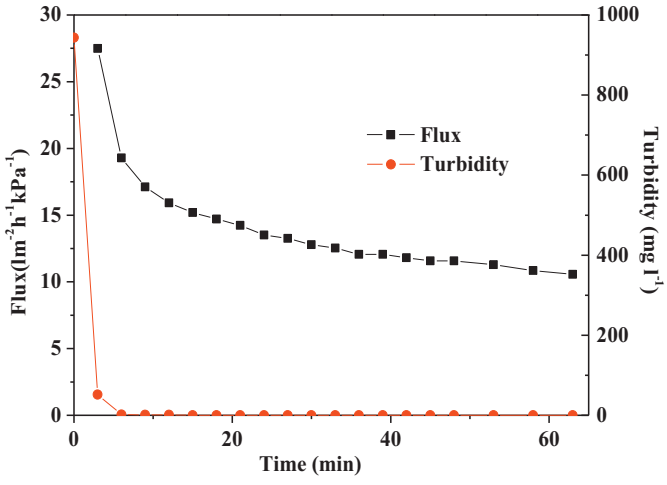

Fig. 7. The flux and turbidity variation with time during the $CaCO_3$ dynamic membrane formation stage (the concentration of $CaCO_3$ was 5.0 g l^{-1}).

There was no turbidity detected at the inflection point on the curve (at 15 min), which indicated the complete formation of dynamic membrane. The pre-coating time was determined using the time interval between the startup time and the time when there was no turbidity in effluent, which was about 15 min in this study. During the pre-coating stage, the dynamic cake layer was formed rapidly and the thickness of the dynamic layer increased continuously, which resulted in the severe flux decline. Once the dynamic membrane was formed, the decline of permeate flux was slow and the turbidity removal for the effluent was completely realized.

3.3.2. The filtration performance of dynamic membrane system

The filtration performances of dynamic membrane and bare membrane in filtrating photocatalysts TiO_2 and Fe-$ZnIn_2S_4$ were carried out in the hybrid system. The concentrations of the photocatalysts TiO_2 and Fe-$ZnIn_2S_4$ were maintained at 1.0 g l^{-1}. The continuously rotating membrane module (dynamic or bare membrane), serving as the stirrer to maintain photocatalysts in suspension, was operated under a permeate flux of 7.6 l m^{-2} h^{-1}. The separation effectiveness of photocatalysts (Fe-$ZnIn_2S_4$ and TiO_2) by dynamic membrane and bare membrane was determined on the basis of turbidity removal. As shown in Fig. 8, the pre-coated dynamic membrane can significantly enhance the filtration performance and improve the rejection of both TiO_2 and Fe-$ZnIn_2S_4$. The rejection of Fe-$ZnIn_2S_4$ by bare membrane was more effective than the rejection of TiO_2, which can be attributed to the larger particle size of Fe-$ZnIn_2S_4$ (3–5 μm, determined from SEM image) than TiO_2 (P25, ~25 nm). All the Fe-$ZnIn_2S_4$ fine particles were rejected by the pre-coated dynamic membrane after 1 h filtration. Though TiO_2 particles were completely rejected after 3.5 h filtration, the effluent turbidity dropped to below 10 mg l^{-1} after 0.5 h filtration. The nano$CaCO_3$ particles initially narrowed and/or partly blocked the supporting membrane pore and resulted in rapid decrease of the flux. Then the deposit particles started to form a cake layer on membrane surface and the formed dynamic membrane determined the rejection properties. Therefore, the pre-coated dynamic membrane can significantly enhance the retention/rejection of photocatalysts.

3.3.3. Photocatalytic dehalogenation in the hybrid system

Control tests with $CaCO_3$ with/without photocatalysts (Fe-$ZnIn_2S_4$ and/or TiO_2) under UV light and the direct photolysis of

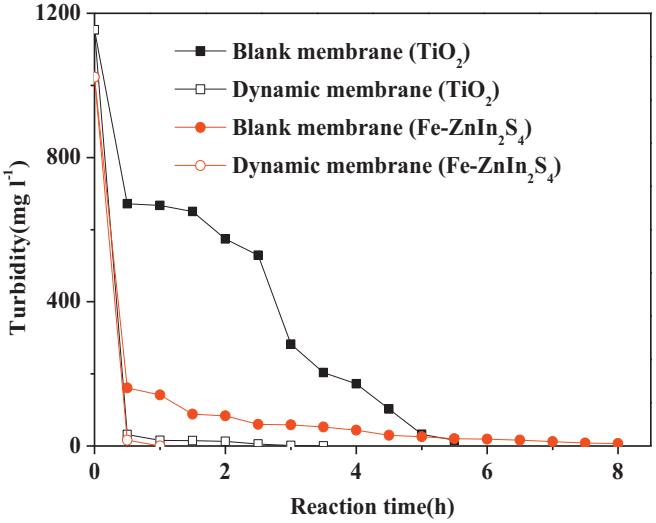

Fig. 8. The rejection rate of photocatalysts by dynamic membrane and blank membrane.

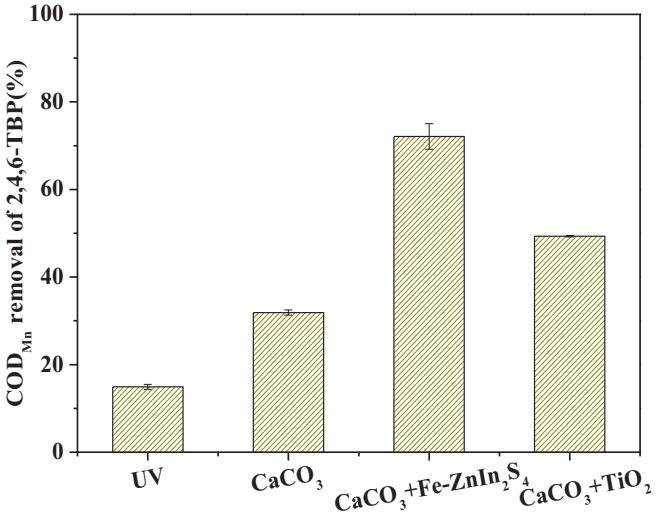

Fig. 10. The COD_{Mn} removal of 2,4,6-TBP in continuous mode.

2,4,6-TBP and 2,4-DCP without $CaCO_3$ and photocatalysts were conducted. The residence time of the solution in the reactor was about 2.0 h. 2,4,6-TBP was completely decomposed when the residence time was kept at 2.0 h and no 2,4,6-TBP was detected in the permeate effluent. The ratios of actually formed Br^- (C) to the formed Br^- at 100% conversion (C_{100}) were shown in Fig. 9. The debromination in the hybrid system remained relatively steady. About 30% bromide ion was released by the direct photolysis (bare membrane without photocatalysts) in the continuous mode, which corresponded with the direct photolysis in batch mode. The dynamic $CaCO_3$ membrane under UV irradiation can realize 50% debromination which is lower than the result (67%) in batch mode. This can be attributed to the dynamic membrane which always shaded part of the solution and reduced UV absorption by the solution than in the suspension system.

In the hybrid photocatalysis and dynamic $CaCO_3$ membrane system, the highest debromination (85–90%) was obtained in the presence of photocatalyst Fe-$ZnIn_2S_4$, which was ~40% higher than TiO_2. It was further demonstrated that Fe-$ZnIn_2S_4$ was very efficient in debromination. Though nano$CaCO_3$ dynamic membrane can assist and improve debromination to some extent, the degree of debromination and mineralization mainly depended on the activity of photocatalysts in continuous mode. As shown in Fig. 10, very high mineralization (72%) also occurred in the hybrid system, which was as high as the COD removal in the batch mode (70%). Both the debromination and mineralization were enhanced in the hybrid system.

Similarly, higher degree dechlorination and mineralization of 2,4-DCP were also achieved in the hybrid system. The degradation rate of 2,4-DCP, the removal ratio of COD and ratios of actually formed Cl^- (C) to the released Cl^- at 100% conversion (C_{100}) were shown in Fig. 11. The blank test of $CaCO_3$ without photocatalyst in the dark removed about 20% 2,4-DCP and there was no Cl^- formed. In the hybrid dynamic membrane system in the absence of photocatalysts, ~95% 2,4-DCP was removed and ~85% Cl^- was formed. When photocatalyst TiO_2 was introduced to the hybrid system, there was 3–5% increase in 2,4-DCP removal (98%) and released Cl^- (90%), also an increase in COD removal (62%). This indicated that $CaCO_3$ played an important role in the hybrid system for degradation of 2,4-DCP, which had been discussed in the batch mode section. Fe doped $ZnIn_2S_4$ exhibited great photocatalytic

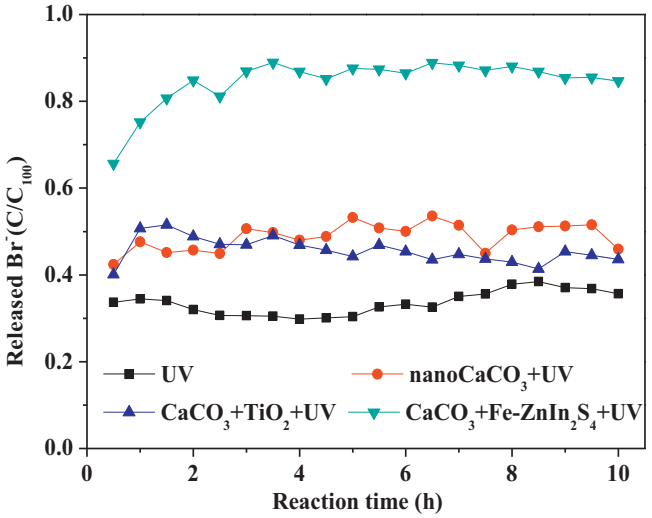

Fig. 9. Photodebromination of 2,4,6-TBP under continuous mode by nano$CaCO_3$ dynamic membrane (retention time 2.0 h, catalyst dosage 1.0 g l^{-1}, [2,4,6-TBP]$_0$ = 40 mg l^{-1}).

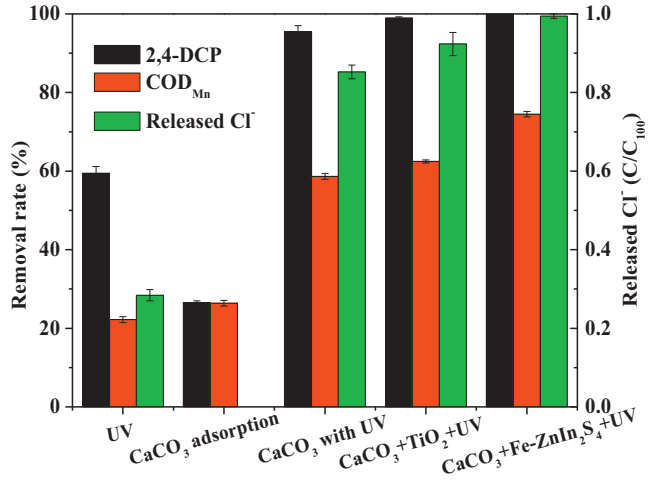

Fig. 11. The removal of 2,4-DCP and COD and the ratios of actually formed Cl^- to be formed Cl^- at 100% dechlorination under continuous mode (HRT = 2.0 h, [2,4-DCP]$_0$ = 15 mg l^{-1}, catalysts dosage 1.0 g l^{-1} C_{100} was the content of Cl^- at 100% dechlorination).

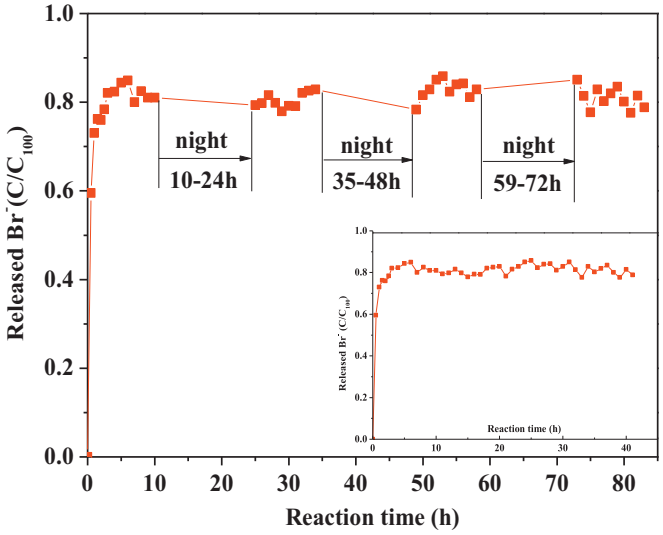

Fig. 12. The efficiency of photodebromination under continuous mode by $CaCO_3$ dynamic membrane for long term photo-debromination (retention time 2.0 h, catalyst dosage 1.0 g l^{-1}, $[2,4,6\text{-TBP}]_0$ = 40 mg l^{-1}).

activity in decomposing 2,4-DCP. When Fe-$ZnIn_2S_4$ was used in the hybrid system, 100% 2,4-DCP removal, 99% Cl^- release and 75% COD removal were achieved.

3.4. Long-term stable operation of the photocatalytic debromination in hybrid photocatalysis and dynamic membrane system

The long-term photocatalytic debromination was carried out to evaluate the stability of the hybrid photocatalysis and dynamic membrane system and reuse of the photocatalyst. The experiment was discontinued during the night.

2,4,6-TBP was completely decomposed during the long term continuous experimental period and no 2,4,6-TBP was detected in the permeate effluent. As shown in Fig. 12, the debromination was maintained at about 85% during the photocatalytic debromination in daytime (total 40 h) which was stopped for the interval at night (total 40 h, the inset in Fig. 12). It was also shown that the interval at night did not affect the photocatalytic activity, and the photocatalyst (Fe-$ZnIn_2S_4$) could be used for a long time without significant loss in photocatalytic activity.

The hybrid photocatalysis and dynamic membrane system was very steady in the long-term operation and the photocatalysts could be completely rejected and turbidity was not detected in the effluent. The long-term experiment indicated that the $CaCO_3$ dynamic membrane and photocatalysis hybrid system might be appropriate for practical application. Once deactivation of the photocatalyst occurred in the hybrid system, fresh photocatalyst can be introduced, when the membrane gets eventually severely fouled, a new dynamic membrane can always be formed and applied.

4. Conclusions

The combination of dynamic membrane ($CaCO_3$) with photocatalysts (Fe-$ZnIn_2S_4$) is proved to be feasible for removal of halogenated compounds in water. This hybrid system can realize continuous photocatalysis, stirring and separation of photocatalysts in a single device. The investment and operational costs are expected to be lower than the conventional PMR system due to the lower costs of supporting membrane materials, abundant $CaCO_3$ and the higher photocatalytic efficiency. The pre-coated dynamic membrane can significantly enhance the filtration performance and improve the rejection of photocatalysts. The dynamic membrane system with Fe-$ZnIn_2S_4$ achieved highest COD removal, dehalogenation efficiencies and complete removal of halogenated compounds in the hybrid PMR system. The long-term photocatalytic debromination experiments demonstrated that the dynamic membrane hybrid system was very steady in the long-term operation and achieved great quality of the permeate effluent. The presence of $CaCO_3$ during UV irradiation could significantly assist and enhance dehalogenation efficiency. The multifunctional performance of the hybrid photocatalysis and dynamic membrane system indicates great application prospect in wastewater treatment.

Appendix A. Supplementary data

Supplementary data associated with this article can be found, in the online version, at http://dx.doi.org/10.1016/j.apcatb.2013.02.023.

References

[1] G. Parshetti, R. Doong, Water Research 45 (2011) 4198–4210.
[2] K. Christoforidis, E. Serestatidoua, M. Louloudib, I. Konstantinoua, E. Milaevac, Y. Deligiannakisa, Applied Catalysis B: Environmental 101 (2011) 417–424.
[3] G. Li, S. Park, D. Kang, R. Krajmalnik-Brown, B. Rittmann, Environmental Science and Technology 45 (2011) 8359–8367.
[4] C. Sun, D. Zhao, C. Chen, W. Ma, J. Zhao, Environmental Science and Technology 43 (2009) 157–162.
[5] J. Xu, W. Meng, Y. Zhang, L. Li, C. Guo, Applied Catalysis B: Environmental 107 (2011) 355–362.
[6] P. Le-Clech, E. Lee, V. Chen, Water Research 40 (2006) 323–330.
[7] X. Huang, M. Leal, Q. Li, Water Research 42 (2008) 1142–1150.
[8] P. Yao, K. Choo, M. Kim, Water Research 43 (2009) 4238–4248.
[9] G. Plantard, V. Goetz, Chemical Engineering and Processing: Process Intensification 62 (2012) 129–136.
[10] S. Mozia, Separation Science and Technology 73 (2010) 71–91.
[11] N. Ma, Y. Zhang, X. Quan, X. Fan, H. Zhao, Water Research 44 (2010) 6104–6114.
[12] N. Ma, X. Quan, Y. Zhang, S. Chen, H. Zhao, Journal of Membrane Science 335 (2009) 58–67.
[13] C.P. Athanasekoua, G.E. Romanosa, F.K. Katsarosa, K. Kordatosb, V. Likodimosa, P. Falarasa, Journal of Membrane Science 392–393 (2012) 192–203.
[14] H. Song, J. Shao, Y. He, B. Liu, X. Zhong, Journal of Membrane Science 405–406 (2012) 48–56.
[15] S. Yang, J. Gu, H. Yu, J. Zhou, S. Li, X. Wu, L. Wang, Separation and Purification Technology 83 (2011) 157–165.
[16] J. Fu, M. Ji, Z. Wang, L. Jin, D. An, Journal of Hazardous materials B131 (2006) 238–242.
[17] V. Augugliaro, E. Lopez, V. Loddo, S. Malato-Rodrguez, I. Maldonado, G. Marc, R. Molinari, L. Palmisano, Solar Energy 79 (2005) 402–408.
[18] G. Zhang, J. Zhang, L. Wang, Q. Meng, J. Wang, Journal of Membrane Science 389 (2012) 532–543.
[19] S. Chin, K. Chiang, A.G. Fane, Journal of Membrane Science 275 (2006) 202–211.
[20] K. Choo, D. Chang, K. Park, M. Kim, Journal of Hazardous Materials 152 (2008) 183–190.
[21] M.J. Benotti, B.D. Stanford, E.C. Wert, S.A. Snyder, Water Research 43 (2009) 1513–1522.
[22] M.E. Ersahin, H. Ozgun, R.K. Dereli, I. Ozturk, K. Roest, J.B. Lier, Bioresource Technology 122 (2012) 196–206.
[23] Y. Pan, T. Wang, H. Sun, W. Wang, Separation and Purification Technology 89 (2012) 78–83.
[24] T. Yang, Z. Ma, Q. Yang, Desalination 270 (2011) 50–56.
[25] B. Gao, L. Liu, J. Liu, F. Yang, Applied Catalysis B: Environmental 129 (2013) 89–97.
[26] L. Liu, B. Gao, J. Liu, F. Yang, Chemical Engineering Journal 181–182 (2012) 486–493.
[27] W. Zhang, X. Li, Z. Qu, Q. Zhao, G. Chen, Materials Letters 64 (2010) 71–73.
[28] A. Gal, V. Brumfeld, S. Weiner, L. Addadi, D. Oron, Advanced Materials 24 (2012) 77–83.